NMR Studies of $Ru_3(CO)_{10}(PMe_2Ph)_2$ and $Ru_3(CO)_{10}(PPh_3)_2$ and Their H_2 Addition Products: Detection of New Isomers with Complex Dynamic Behavior

Damir Blazina,[†] Simon B. Duckett,*[,†] Paul J. Dyson,*[,†] Brian F. G. Johnson,*[,‡] Joost A. B. Lohman,[§] and Christopher J. Sleigh[†]

Contribution from the Department of Chemistry, University of York, Heslington, York YO10 5DD, U.K., University Chemistry Laboratory, Lensfield Road, Cambridge CB2 1EW, U.K., and Bruker UK Limited, Banner Lane, Coventry CV4 9GH, U.K.

Received December 12, 2000. Revised Manuscript Received June 6, 2001

Abstract: The clusters $Ru_3(CO)_{10}L_2$, where L = PMe_2Ph or PPh_3, are shown by NMR spectroscopy to exist in solution in at least three isomeric forms, one with both phosphines in the equatorial plane on the same ruthenium center and the others with phosphines in the equatorial plane on different ruthenium centers. Isomer interconversion for $Ru_3(CO)_{10}(PMe_2Ph)_2$ is highly solvent dependent, with $\Delta H^{\ddagger}$ decreasing and $\Delta S^{\ddagger}$ becoming more negative as the polarity of the solvent increases. The stabilities of the isomers and their rates of interconversion depend on the phosphine ligand. A mechanism that accounts for isomer interchange involving Ru−Ru bond heterolysis is suggested. The products of the reaction of $Ru_3(CO)_{10}L_2$ with hydrogen have been monitored by NMR spectroscopy via normal and para hydrogen-enhanced methods. Two hydrogen addition products are observed with each containing one bridging and one terminal hydride ligand. EXSY spectroscopy reveals that both *intra-* and *inter*isomer hydride exchange occurs on the NMR time scale. On the basis of the evidence available, mechanisms for hydride interchange involving Ru−Ru bond heterolysis and CO loss are proposed.

Introduction

Since transition metal carbonyl clusters represent an intermediate state between mononuclear complexes and colloids/nanoparticles they have been widely studied over the last 30 years.[1] In particular, organic substrates are able to adopt multicenter bonding modes with clusters that profoundly influence their subsequent reactivity.[2] Recently, this has enabled organic transformations to be completed that are not possible by mononuclear homogeneous catalysts.[3] The ability of a species to access a degree of electronic unsaturation remains a key step in such processes. While homogeneous mononuclear complexes tend to achieve this by ligand dissociation, clusters may employ other processes, including fragmentation, polyhedral transformations, and the activation of multiple metal−metal bonds.

Triruthenium dodecacarbonyl and its phosphine (L) derivatives $Ru_3(CO)_{12-n}L_n$ (where n = 1−3) have been shown to catalyze numerous hydrogenation and hydroformylation reactions.[4,5] The X-ray crystal structures of several phosphine derivatives have been reported for ruthenium and osmium clusters of this type,[4−7] and both conformational and structural isomers have been observed with the osmium clusters.[8,9] In these structures, the phosphine ligands are restricted to equatorial locations. While X-ray crystallography remains the main tool for elucidating the structure of clusters, their stereochemical nonrigid behavior is studied most readily by NMR spectroscopy.[10]

The substitution chemistry of $Ru_3(CO)_{12-x}L_x$ has been studied by a number of groups.[11−16] Simple substitution has been

[†] University of York.
[‡] University Chemistry Laboratory.
[§] Bruker UK Ltd.

(1) For example, see: (a) *Transition Metal Clusters*; Johnson, B. F. G., Ed.; Wiley: Chichester, U.K., 1980. (b) *Catalysis by Di- and Polynuclear Metal Cluster Complexes*; Adams R. D., Cotton F. A., Eds.; Wiley-VCH: New York, 1998. (c) *Metal Clusters in Chemistry*; Braunstein, P., Oro, L. A., Raithby, P. R., Eds.; Wiley-VCH: New York, 1999. (d) Dyson, P. J.; McIndoe, J. S. *Transition Metal Carbonyl Cluster Chemistry*; Gordon and Breach: Amsterdam, 2000.

(2) Adams, R. D. In *The Chemistry of Metal Cluster Complexes*; Shriver, D. F., Kaesz, H. D., Adams, R. D., Eds.; Wiley-VCH: New York, 1990.

(3) For example, see: (a) Kondo, T.; Akazome, M.; Tsuji, Y.; Watanabe, Y. *J. Org. Chem.* **1990**, *55*, 1286. (b) Chatani, N.; Ie, Y.; Kakiuchi, F.; Murai, S. *J. Org. Chem.* **1997**, *62*, 2604. (c) Ishii, Y.; Chatani, N.; Kakiuchi, F.; Murai, S. *Organometallics* **1997**, *16*, 3615. (d) Chatani, N.; Ishii, Y.; Ie, Y.; Kakituchi, F.; Murai, S. *J. Org. Chem.* **1998**, *63*, 5129.

(4) Gervasio, G.; Giordano, R.; Marabello, D.; Sappa, E. *J. Organomet. Chem.* **1999**, *588*, 83.

(5) (a) Fontal, B.; Reyes, M.; Suárez, T.; Bellandi, F.; Díaz, J. C. *J. Mol. Catal. A.* **1999**, *149*, 75. (b) Fontal, B.; Reyes, M.; Suárez, T.; Bellandi, F.; Ruiz, N. *J. Mol. Catal. A.* **1999**, *149*, 87.

(6) Bruce, M. I.; Matisons, J. G.; Nicholson, B. K. *J. Organomet. Chem.* **1983**, *247*, 321.

(7) (a) Bruce, M. I.; Skelton, B. W.; White, A. H.; Zaitseva, N. N. *Aust. J. Chem.* **1997**, *50*, 163. (b) Bruce, M. I.; Liddell, M. J.; Hughes, C. A.; Patrick, J. M.; Skelton, B. W.; White, A. H. *J. Organomet. Chem.* **1988**, *347*, 181.

(8) Hansen, V. M.; Ma, A. K.; Biradha, K.; Pomeroy, R. K.; Zaworotko, M. J. *Organometallics* **1998**, *17*, 5267.

(9) (a) Deeming, A. J.; Donovan-Mtunzi, S.; Kabir, S. E.; Manning, P. J. *J. Chem. Soc., Dalton Trans.* **1985**, 1037. (b) Leong, W. K.; Liu, Y. *J. Organomet. Chem.* **1999**, *584*, 174.

(10) Dolgushin, F. M.; Grachova, E. V.; Heaton, B. T.; Iggo, J. A.; Koshevoy, I. O.; Podkorytov, I. S.; Smawfield, D. J.; Tunik, S. P.; Whyman, R.; Yanovskii, A. I. *J. Chem. Soc., Dalton Trans.* **1999**, 1609.

(11) Keeton, D. P.; Malik, S. K.; Poë, A. *J. Chem. Soc., Dalton Trans.* **1977**, 233.

(12) Chen, L.; Poë, A. *Can. J. Chem.* **1989**, *67*, 1924.

(13) Johnson, B. F. G. *Inorg. Chim. Acta* **1986**, *115*, L39.

(14) Adams, H.; Bailey, N. A.; Bentley, G. W.; Mann, B. E. *J. Chem. Soc., Dalton Trans.* **1989**, 1831.

10.1021/ja004245n CCC: $20.00
Published on Web 09/12/2001

proposed to occur via dissociative pathways, but competing formation of mononuclear products such as $Ru(CO)_4L$ and $Ru(CO)_3L_2$ results in highly complex reaction systems. These studies have involved kinetic measurements and the rationalization of activation parameter data. For example, the substitution of PPh_3 in $Ru_3(CO)_9(PPh_3)_3$ has been shown to follow a pathway that involves reversible PPh_3 loss with competing CO loss and homolytic Ru−Ru bond fission.[11] The latter process leads to fragmentation and the initial formation of mono- and binuclear products. Consistently low values of $\Delta S^{\ddagger}$ for the dissociative route have been explained by invoking reorganization of the 46-electron intermediate $Ru_3(CO)_{10}L$ such that an 18-electron count is obtained at each metal center.[12] It has also been proposed that these three pathways could be preceded by common, and reversible, fission of a single Ru−Ru bond.[11] Alternative mechanisms for CO substitution in $M_3(CO)_{12-x}L_x$ (where M = Fe, Ru, Os and $x = 0, 1, 2$) have been suggested, which invoke both heterolytic fission of a M−M bond[13] and merry-go-round exchange.[14,15] Similar mechanisms have been proposed for $MM'(CO)_{10}$ (where M = M′ = Mn, Re; M = Mn; and M′ = Re)[16] as well as for $Ir_4(CO)_{12-n}L_n$ ($n = 0-3$).[17,18]

The reactivity of such clusters toward hydrogen and their catalytic activity has also been investigated.[1,19] One high-sensitivity NMR technique that has recently been developed to probe the role that metal hydride complexes play in catalytic transformations involves the use of para hydrogen (p-H_2). This phenomenon, initially termed the PASADENA effect,[20] now usually called para hydrogen-induced polarization (PHIP), has been extensively reviewed.[21] Notable achievements include the demonstration that the non-Boltzmann population generated by PHIP enhances scalar-coupled ^{31}P and ^{13}C heteronuclei by cross-relaxation[22] and cross-polarization,[23] the development of selective excitation of polarization by Bargon et al. to remove the need for $\pi/4$ pulse excitation,[24,25] and the use of 2D methods to facilitate the rapid indirect observation of insensitive nuclei.[26,27] Although applications of p-H_2 to cluster chemistry are much less common, Aime et al. have demonstrated that $H_2Os_3(CO)_{10}$, a species with magnetically equivalent hydrides, can be enhanced.[28] The enhanced hydride signal arises via the involvement of an intermediate with inequivalent hydrides. Studies involving $Ru_3(CO)_{11}(NCMe)$ yield an enhanced emission signal for molecular hydrogen that indicated the reversible interaction of p-H_2 with the Ru_3 cluster containing inequivalent hydrides.[29] We previously used p-H_2 to detect new H_2 addition products of $Ru_3(CO)_9(PPh_3)_3$.[30] Here we describe studies on the fluxional behavior of $Ru_3(CO)_{10}(L)_2$, where L = PMe_2Ph or PPh_3, and the detection and characterization of their hydrogen addition products.

Experimental Section

General Methods and Chemicals. All reactions were carried out under nitrogen using glovebox, high-vacuum, or Schlenk line techniques. Subsequent purifications were carried out without precautions to exclude air. Triphenylphosphine and dimethylphenylphosphine (Aldrich), $Ru_3(CO)_{12}$ (Strem Chemicals), hydrogen (99.99%, BOC), and ^{13}CO (99.9%, BP) were used as received. Tetrahydrofuran (THF) was dried over sodium prior to use. The clusters $Ru_3(CO)_{10}(PMe_2Ph)_2$ **1** and $Ru_3(CO)_{10}(PPh_3)_2$ **2** were prepared according to literature methods[31] and purified on a silica column with 80:20 hexane/dichloromethane as the eluent. The mixed phosphine cluster $Ru_3(CO)_{10}(PMe_2Ph)(PPh_3)$ was prepared from $Ru_3(CO)_{11}(PPh_3)$ by reaction with PMe_2Ph, in a manner analogous to that used by Farrar and Lunniss for triiron clusters.[32] Initial characterization was based on IR spectroscopy (ν_{CO}, recorded on a Mattson Unicam Research Series FT-IR instrument) and on FAB mass spectroscopy (performed on a VG Autospec instrument) with observations in excellent agreement with the literature data. Full characterization was achieved using NMR spectroscopy (see later). Labeling of $Ru_3(CO)_{10}(PMe_2Ph)_2$ with ^{13}CO was achieved by stirring a solution of 50 mg of the cluster in THF overnight under an atmosphere of ^{13}CO. This procedure was repeated three times to ensure essentially complete ^{13}CO labeling.

All NMR solvents (Apollo Scientific) were dried using appropriate methods and degassed prior to use. The NMR measurements were made on NMR tubes fitted with J. Young Teflon valves, and solvents were added by vacuum transfer on a high-vacuum line. For the PHIP experiments, hydrogen enriched in the para spin state was prepared by cooling H_2 to 77 K over a paramagnetic catalyst (Fe_2O_3) as described previously.[33] An atmosphere of H_2 equivalent to ~3 atm pressure at 298 K was first introduced into an NMR tube cooled in liquid nitrogen. Samples were thawed immediately prior to introduction into the NMR spectrometer. All NMR spectra were recorded on Bruker DRX-400 spectrometers with ^1H at 400.13 MHz, ^{31}P at 161.9 MHz, and ^{13}C at 100 MHz, respectively. ^1H NMR chemical shifts are reported in ppm relative to residual ^1H signals in the deuterated solvents (benzene-d_5, δ 7.13; toluene-d_7, δ 2.13; $CHCl_3$, δ 7.27; THF-d_7, δ 1.73; nitromethane-d_2, δ 4.33), ^{31}P NMR in ppm downfield of an external 85% solution of phosphoric acid, and ^{13}C NMR relative to benzene-d_6, δ 128.0, and toluene-d_8, δ 21.3. Normal and modified COSY,[27] HMQC,[34] and EXSY[35] pulse sequences were used as previously described.

Dynamic Methods for Complexes 1 and 2. The ^{31}P EXSY spectra were analyzed according to literature methods.[36] The rate of phosphine

(15) Adams, H.; Agustinho, C. M.; Mann, B. E.; Smith, S. *J. Organomet. Chem.* **2000**, *607*, 175.
(16) Johnson, B. F. G. *J. Organomet. Chem.* **1991**, *415*, 109.
(17) Johnson, B. F. G.; Roberts, Y. *Inorg. Chim. Acta* **1993**, *205*, 175.
(18) (a) Mann, B. E.; Pickup, B. T.; Smith, A. K. *J. Chem. Soc., Dalton Trans.* **1989**, 889. (b) Mann, B. E.; Vargas, M. D.; Khadar, R. *J. Chem. Soc., Dalton Trans.* **1992**, 1725.
(19) (a) Cabeza, J. A.; Fernandez-Colinas, J. M.; Llamazares, A.; Riega, V. *Organometallics* **1993**, *12*, 4141. (b) Castiglioni, M.; Deabate, S.; Giordano, R.; King, P. J.; Knox, S. A. R.; Sappa, E. *J. Organomet. Chem.* **1998**, *571*, 251. (c) Gervasio, G.; Giordano, R.; Marabello, D.; Sappa, E. *J. Organomet. Chem.* **1999**, *588*, 83. (d) Süss-Fink, G.; Meister, G. *Adv. Organomet. Chem.* **1993**, *35*, 41.
(20) Bowers, C. R.; Weitekamp, D. P. *J. Am. Chem. Soc.* **1987**, *109*, 5541.
(21) (a) Bowers, C. R.; Jones, D. H.; Kurur, N. D.; Labinger, J. A.; Pravica, M. G.; Weitekamp, D. P. *Adv. Magn. Reson.* **1990**, *14*, 269. (b) Natterer, J.; Bargon, J. *Prog. Nucl. Magn. Reson. Spectrosc.* **1997**, *31*, 293. (c) Duckett, S. B.; Sleigh, C. J. *Prog. Nucl. Magn. Reson. Spectrosc.* **1999**, *34*, 71.
(22) (a) Eisenschmid, T. C.; McDonald, J.; Eisenberg, R.; Lawler, R. G. *J. Am. Chem. Soc.* **1989**, *111*, 7267. (b) Barkemeyer, J.; Haake, M.; Bargon, J. *J. Am. Chem. Soc.* **1995**, *117*, 2927.
(23) (a) Duckett, S. B.; Newell, C. L.; Eisenberg, R. *J. Am. Chem. Soc.* **1993**, *115*, 1156. (b) Haake, M.; Natterer, J.; Bargon, J. *J. Am. Chem. Soc.* **1996**, *118*, 8688.
(24) Barkemeyer, J.; Bargon, J.; Sengstschmid, H.; Freeman, R. *J. Magn. Reson. Ser. A* **1996**, *120*, 129.
(25) Sengstschmid, H.; Freeman, R.; Barkemeyer, J.; Bargon, J. *J. Magn. Reson. Ser. A* **1996**, *120*, 249.
(26) (a) Duckett, S. B.; Barlow, G. K.; Partridge, M. G.; Messerle, B. A. *J. Chem. Soc., Dalton. Trans.* **1995**, 3427. (b) Duckett, S. B.; Mawby, R. J.; Partridge, M. G. *J. Chem. Soc. Chem. Commun.* **1996**, 383. (c) Millar, S. P.; Jang, M.; Lachicotte, R. J.; Eisenberg, R. *Inorg. Chim. Acta* **1998**, *270*, 363.
(27) Messerle, B. A.; Sleigh, C. J.; Partridge, M. G.; Duckett, S. B. *J. Chem. Soc., Dalton Trans.* **1999**, 1429.
(28) Aime, S.; Gobetto, R.; Canet, D. *J. Am. Chem. Soc.* **1998**, *120*, 6770.
(29) Aime, S.; Dastru, W.; Gobetto, R.; Russo, A.; Viale, A.; Canet, D.; *J. Phys. Chem. A.* **1999**, *103*, 9702.
(30) Sleigh, C. J.; Duckett, S. B.; Mawby, R. J.; Lowe, J. P. *Chem. Commun.* **1999**, 1223.
(31) (a) Bruce, M. I.; Kehoe, D. C.; Matisons, J. G.; Nicholson, B. K.; Reiger, H. R.; Williams, M. L. *J. Chem. Soc. Chem. Commun.* **1982**, 442. (b) Bruce, M. I.; Matisons, J. G.; Nicholson, B. K. *J. Organomet. Chem.* **1983**, *247*, 321.
(32) Farrar, D. H.; Lunniss, J. A. *J. Chem. Soc., Dalton Trans.* **1987**, 1249.
(33) Duckett, S. B.; Newell, C. L.; Eisenberg, R. *J. Am. Chem. Soc.* **1994**, *116*, 10548.
(34) (a) Aue, W. P.; Bartholdi, E.; Ernst, R. R. *J. Chem. Phys.* **1976**, *64*, 2229. (b) Nagayama, K.; Kumar, A.; Wüthrich, K.; Ernst, R. R. *J. Magn. Reson.* **1980**, *40*, 321.

exchange, k/s^{-1}, was determined according to eq 1, where t_m represents

$$k = \frac{1}{t_m} \ln\left(\frac{I+1}{I-1}\right) \quad (1)$$

the mixing time and I the ratio of intensities of the diagonal and exchange cross-peaks. Suitable plots enable $k_{forward}$ and $k_{reverse}$ to be determined from the gradient. This analysis is normally used for simple two-site exchange but has been used here to determine $k_{forward}$ and $k_{reverse}$ even though the populations of the two sites are not the same. The apparent relaxation times of the ^{31}P centers were found to be identical ($T_1 = 0.28$ s) within experimental error.

At high temperatures, the process became too fast to be monitored by the EXSY route. Quantitative ^{31}P spectra were then acquired and line-shape fitting, performed using the gNMR program version 4.0.1 (Cherwell Scientific), yielded the rate constants. The experiment was repeated over a range of temperatures, and the activation parameters $\Delta H^{\ddagger}$ and $\Delta S^{\ddagger}$ were determined by nonlinear regression using SPSS for Windows version 9.0.

Dynamic Methods for Complex 3. To monitor hydride ligand exchange in **3**, a series of 2D gradient-assisted EXSY spectra were recorded.[27] In a typical run, data were collected at selected temperatures for a series of mixing times τ (usually 25, 50, 75, 200, 400, 600, and 800 ms). The sum of the integrals of the diagonal peak areas for a given hydride location and the cross-peak areas arising due to exchange were then normalized to 100%. The rate of site exchange was then determined by simulation; the change in intensity of the signal at a given hydride position (100 when $\tau = 0$) was modeled as a function of τ. This was carried out using Microsoft Excel 97. The peak intensities were calculated for 0.01 s intervals from 0.01 s to τ_{max} and those for each experimentally observed time were then compared with the experimental values via a minimized linear least-squares difference analysis.[37] The associated rate constants were varied until the sum of the squares of the difference between measured and simulated points was minimized. Rate constants obtained in this way were multiplied by a factor of 2 to take into account the analysis method.[38]

Kinetic Model. To model the hydride exchange process, the following assumptions were made: the rate of hydride exchange within an isomer is the same for both terminal → bridge and bridge → terminal processes. Likewise, for isomer exchange, the rate of transfer of both hydrides must be the same. The magnitude of the following rate constants were obtained by simulation of the EXSY data: (i) *intra*molecular hydride exchange within **3a**, i.e., **3a***b* → **3a***t* and reverse; (ii) *intra*molecular hydride exchange within **3b**, i.e., **3b***b* → **3b***t* and reverse; (iii) *inter*molecular hydride exchange from **3a** to **3b**, keeping original hydride position, i.e., **3a***b* → **3b***b* and **3a***t* → **3b***t*; (iv) *inter*molecular hydride exchange from **3a** to **3b** with hydride position interchange, i.e., **3a***b* → **3b***t* and **3a***t* → **3b***b*; (v) the reverse of processes iii and iv.

Results and Discussion

Characterization of $Ru_3(CO)_{10}(PMe_2Ph)_2$ and $Ru_3(CO)_{10}(PPh_3)_2$. Clusters $Ru_3(CO)_{10}(PMe_2Ph)_2$ **1** and $Ru_3(CO)_{10}(PPh_3)_2$ **2**, prepared using literature methods, produced mass spectra and IR data that matched those expected.[31] ^1H NMR data for **1** and **2** were also found to agree with those reported previously.[31] Surprisingly, the $^{31}P\{^1H\}$ NMR spectrum of **1** in toluene-d_8 at 301 K consisted of two singlets at δ −0.95 and −2.3 in the ratio 1:0.67. These signals coalesce at 344 K. While these data confirm the identity of **1** as $Ru_3(CO)_{10}(PMe_2Ph)_2$, they indicate the presence of two phosphine environments and hence more than one structural form. While the resonance at δ −2.3 was unaffected by cooling below 301 K, the peak at δ −0.95 split into two equally intense signals at δ 1.55 and −4.77 and 189 K. These two signals coalesced at 208 K, with line shape analysis indicating that the associated rate constant for ligand interchange is 90 s^{-1}.

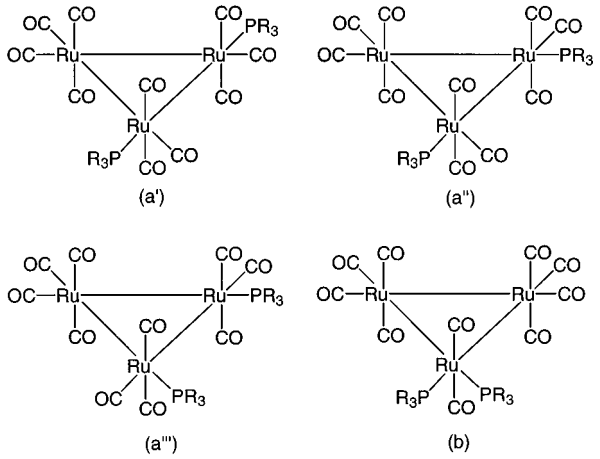

Figure 1. Structures of $Ru_3(CO)_{10}(PR_3)_2$ with two equatorial phosphine ligands (PR_3 = PMe_2Ph or PPh_3). Arrangement **a′** corresponds to the solid-state structure found in the literature.[7]

In the case of **2**, the corresponding ^{31}P NMR spectrum at 301 K contains a broad singlet at δ 36.5, while at 253 K two resonances are detected (δ 36.1 and 37.9) with relative intensity 1:0.63 (peak coalescence at 265 K). Upon cooling to 189 K, the signal at δ 36.1 splits again into two equally intense signals at δ 42.7 and 36.7. This information suggests that **2** also exists as a set of rapidly interconverting isomers. Since literature evidence indicates that axial phosphine arrangements are unprecedented,[39] the four structures shown in Figure 1 might be expected (form **a′** matches that reported in the solid state).[7,31]

To learn more about **1** and **2**, the mixed phosphine cluster $Ru_3(CO)_{10}(PMe_2Ph)(PPh_3)$ was prepared. ^{31}P NMR investigation of this sample indicated the presence of a 1:1:3 ratio of **1**:**2**: $Ru_3(CO)_{10}(PMe_2Ph)(PPh_3)$ at 296 K, of which the signals for $Ru_3(CO)_{10}(PMe_2Ph)(PPh_3)$ corresponded to a pair of coupled resonances at δ −1.5 (d, $J_{(PP)}$ 9.8 Hz, PMe_2Ph, 275 K) and 36.9 (d, $J_{(PP)}$ 9.8 Hz, PPh_3) and two further singlets at δ −0.86 and 38.5. Since the coupled signals are connected by an NOE interaction in the appropriate NMR experiment at 203 K the associated phosphine ligands must be located on the same Ru center (structure **b** from Figure 1). Furthermore, both the two additional resonances split into equally intense signals at δ 0.42 and −4.88 (PMe_2Ph) and δ 40.67 and 40.91 (PPh_3), respectively, at 189 K. Unfortunately, since structural forms **a′**, **a″**, and **a‴** contain just two distinct trans phosphine arrangements, namely, $R_3P-Ru-Ru-CO$ and $R_3P-Ru-Ru-PR_3$, only two ^{31}P signals might be expected for these three isomers.[40] The spectral features described here are therefore consistent with the observation of structure **b** and at least two of the remaining three isomers. It is also worth noting that while very rapid interisomer exchange is observed, interspecies exchange between **1**, **2**, and $Ru_3(CO)_{10}(PMe_2Ph)(PPh_3)$ was not seen.

Ligand Exchange Pathways in $Ru_3(CO)_{10}(PMe_2Ph)_2$ and $Ru_3(CO)_{10}(PPh_3)_2$. The change in appearance of the ^{31}P NMR signals of **1** as a function of temperature revealed that interconversion occurs between the isomers with phosphine ligands on different ruthenium centers (**1a′**, **1a″**, **1a‴**).[41] However, these

(35) Bax, A.; Griffey, R. H.; Hawkins, B. L. *J. Magn. Reson.* **1983**, *55*, 301.
(36) Bodenhausen, G.; Ernst, R. R. *J. Am. Chem. Soc.* **1982**, *104*, 1304.
(37) Jones, W. D.; Rosini, G. P.; Maguire, J. A. *Organometallics* **1999**, *18*, 1754.
(38) Green, M. L. H.; Wong, L. L.; Sella, A. *Organometallics* **1992**, *11*, 2660.
(39) Deeming, A. J. In *Comprehensive Organometallic Chemistry II*; Abel, E. W., Stone, F. G. A., Wilkinson, G., Eds.; Pergamon Press: Oxford, U.K., 1995; Vol. 7.
(40) Tolman, C. A. *Chem. Rev.* **1977**, *77*, 313.

Table 1. Typical Rate and Equilibrium Constants for the Slower Dynamic Processes in **1** and **2** in $CDCl_3$ as Determined by NMR Methods

	temp (K)							
	223	228	238	244	285	289	296	301
$k_{1a\rightarrow1b}$ (s^{-1})					15.9	22.8	31.1	39.3
$k_{1b\rightarrow1a}$ (s^{-1})					11.0	15.3	20.1	24.9
$K_{1a\rightarrow1b}$					1.88	1.92	1.97	2.02
$k_{2a\rightarrow2b}$ (s^{-1})	0.8	2.6	8.4	16.9				
$k_{2b\rightarrow2a}$ (s^{-1})	0.6	1.9	9.3	17.9				
$K_{2a\rightarrow2b}$	1.09	1.01	0.97	0.90				

processes were too fast to be accurately monitored. Exchange between the signals of **1a** and **1b** has been monitored by 2D ^{31}P-EXSY spectroscopy[35] and line shape analysis.[36] To clarify the mechanism of exchange, this process was monitored in four solvents, toluene-d_8, $CDCl_3$, THF-d_8, and nitromethane-d_3. ^{31}P peak integrations from quantitative measurements were used to obtained K, the equilibrium constant, and the equilibrium parameters $\Delta H^{\varnothing}$ and $\Delta S^{\varnothing}$ via a Van't Hoff analysis. Interestingly, the equilibrium position at 301 K showed a slight solvent dependence, with the integrated peak ratios of **1a** to **1b** changing from 1.54 in toluene-d_8 through 1.96 in THF-d_8 and 2.08 in $CDCl_3$ to 2.26 in nitromethane-d_3. Similar NMR methods have been used to explore the dynamic behavior of **2**. Selected rate and equilibrium constants for the dynamic behavior of **1** and **2** are listed in Table 1, while the activation and equilibrium parameters for interconversion are given in Table 2.

The free energy difference between the averaged forms of **1a** and isomer **1b** obtained from these data is only 1.03 kJ mol^{-1} at 301 K in toluene-d_8. This information is summarized in the reaction coordinate versus free energy plot illustrated in Figure 2. Furthermore, the slight solvent dependence of the equilibrium position (1.54 in toluene-d_8, 1.96 in THF-d_8, 2.08 in $CDCl_3$, and 2.26 in nitromethane-d_3), and the change in $\Delta H^{\varnothing}$ of only 5 kJ mol^{-1}, suggest that the relative stability of these species is only slightly affected by the solvent.

In contrast, the effect of the solvent on the rate constant for isomer interchange is dramatic. Overall, the associated entropy of activation for the **1a** → **1b** process changes from −25 J K^{-1} mol^{-1} in toluene through −64 J K^{-1} mol^{-1} in THF-d_8 and −85 J K^{-1} mol^{-1} in $CDCl_3$ to −105 J K^{-1} mol^{-1} in nitromethane-d_3. The reverse process, **1b** → **1a**, shows a similar trend. These data suggest that the solvent participates in the exchange process, a hypothesis that is supported by the associated decrease in $\Delta H^{\ddagger}$. The total change in bond energy up to the rate-limiting step for this interconversion is therefore clearly reduced by the introduction of a bonding interaction with the solvent, and initial ligand loss can be excluded since a large positive entropy of activation would result. These values are consistent with the findings of Chen and Poë, where $\Delta S^{\ddagger}$ for dissociative CO loss in triruthenium clusters is positive and $\Delta H^{\ddagger}$ far in excess of those found here.[12]

Further support for a nondissociative pathway comes from the fact that when the process was studied in $CDCl_3$ at 285 K neither excess CO (1 atm) nor excess PMe_2Ph (∼120-fold excess) had any effect on the observed exchange rate constants. On moving to toluene-d_8, excess CO again had no effect, whereas added PMe_2Ph led to the rapid formation of $Ru_3(CO)_9(PMe_2Ph)_3$. Fortunately, the corresponding $^{31}P\{^1H\}$ spectrum contained separate signals for **1a** and **1b**, with line shapes and relative intensities identical to those observed in the absence of phosphine. Thus, the addition of neither CO nor phosphine affects the exchange pathway in toluene. This is consistent with the failure to observe interspecies exchange when the mixture of **1**, **2**, and $Ru_3(CO)_{10}(PMe_2Ph)(PPh_3)$ was studied.

Several options still exist for the exchange pathway. However, since the phosphine ligands are restricted to nonaxial sites, their presence eliminates the merry-go-round option.[39,42] Mechanisms involving initial Ru−Ru bond cleavage, via homolytic and heterolytic steps, remain. Homolytic fission, is however, very unlikely because of the dramatic solvent participation[43] *and* the fact that *p*-H_2 enhancements are observed for the corresponding H_2 addition products described later. Heterolytic activation would lead to the generation of an "ionic pair" with one 16-, and two 18-, electron ruthenium centers. This process has already been suggested to account for the substitution chemistry of a wide variety of systems containing metal−metal bonds.[43] The stability of the transition state in such a transformation would be highly solvent dependent. We conclude that the most likely exchange pathway therefore involves such a process, as illustrated in Scheme 1. After the rate-determining step, further ligand rearrangement is necessary, with stepwise movement of the phosphine, followed by CO, or concerted movement of both ligands necessary to re-form **1**. The kinetic and thermodynamic parameters described here provide no information for these steps.

The equilibrium constant connecting structures **2a** and **2b**, where L = PPh_3, is of the same order of magnitude as those found for **1**. Furthermore, the values obtained for the difference in isomer free energy and the associated activation enthalpies are similar. This indicates that there is little steric cost to placing two triphenylphosphine ligands on the same ruthenium center in an equatorial arrangement. There is, however, a notable difference in the effect of solvent on the entropy of activation for isomer interconversion since the values are now essentially zero. This requires significantly reduced levels of solvent participation in rate-determining Ru−Ru bond heterolysis. Since PMe_2Ph is the better electron donor and hence more able to

Table 2. Thermodynamic and Kinetic Data for Slower Isomer Interchange in **1** and **2**

process	variable	toluene-d_8	THF-d_8	$CDCl_3$	CD_3NO_2
1a → **1b**	$\Delta H^{\varnothing}$ (kJ mol^{-1})	5 ± 1	2.3 ± 0.3	3.2 ± 0.3	7 ± 1
(equilibrium)	$\Delta S^{\varnothing}$ (J K^{-1} mol^{-1})	20 ± 5	1 ± 1	15 ± 1	19 ± 4
	$\Delta G^{\varnothing}_{301}$ (kJ mol^{-1})	1.03 ± 0.05	1.33 ± 0.03	1.76 ± 0.05	2.04 ± 0.04
1a → **1b**	$\Delta H^{\ddagger}$ (kJ mol^{-1})	56 ± 7	46 ± 3	39 ± 3	34 ± 3
	$\Delta S^{\ddagger}$ (J K^{-1} mol^{-1})	−25 ± 24	−64 ± 10	−85 ± 10	−105 ± 10
1b → **1a**	$\Delta H^{\ddagger}$ (kJ mol^{-1})	54 ± 4	38 ± 4	34 ± 3	30 ± 2
	$\Delta S^{\ddagger}$ (J K^{-1} mol^{-1})	−29 ± 12	−86 ± 13	−104 ± 11	−114 ± 6
2a → **2b**	$\Delta H^{\varnothing}$ (kJ mol^{-1})	8 ± 1		4 ± 1	
(equilibrium)	$\Delta S^{\varnothing}$ (J K^{-1} mol^{-1})	30 ± 6		18 ± 4	
	$\Delta G^{\varnothing}_{301}$ (kJ mol^{-1})	0.72 ± 0.02		1.23 ± 0.06	
2a → **2b**	$\Delta H^{\ddagger}$ (kJ mol^{-1})	49 ± 3		54 ± 3	
	$\Delta S^{\ddagger}$ (J K^{-1} mol^{-1})	−14 ± 13		0 ± 11	
2b → **2a**	$\Delta H^{\ddagger}$ (kJ mol^{-1})	46 ± 2		52 ± 2	
	$\Delta S^{\ddagger}$ (J K^{-1} mol^{-1})	−35 ± 8		−8 ± 8	

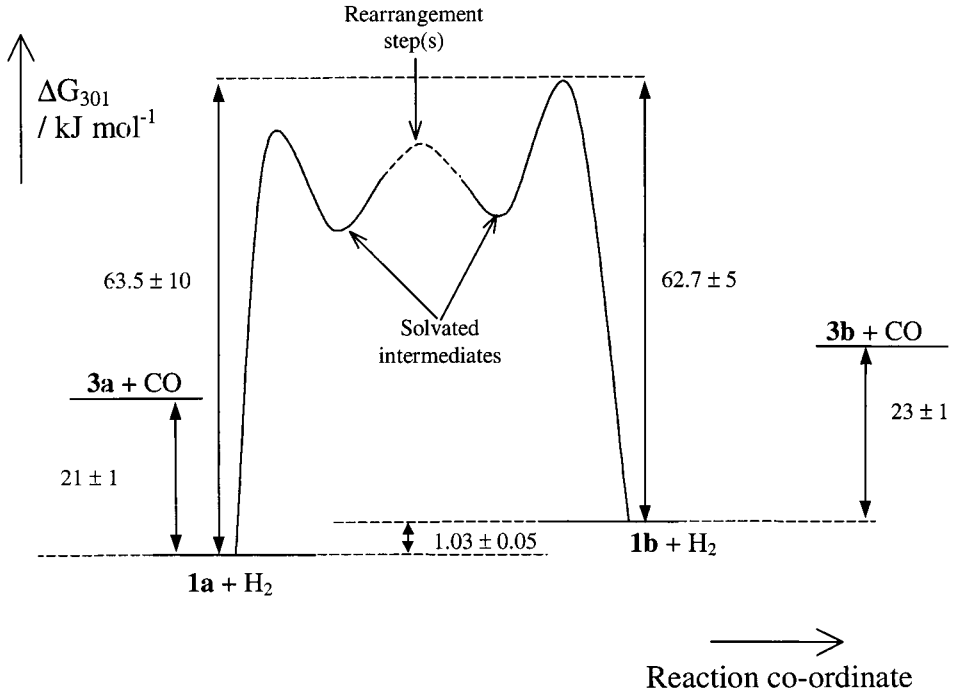

Figure 2. Free energy vs reaction coordinate diagram for **1** and **3** in toluene-d_8 at 301 K. The free energies of activation for interchange of **1a**[41] and **1b** are included.

Scheme 1. Proposed Mechanism for Isomer Exchange from **1a′** to **1b**

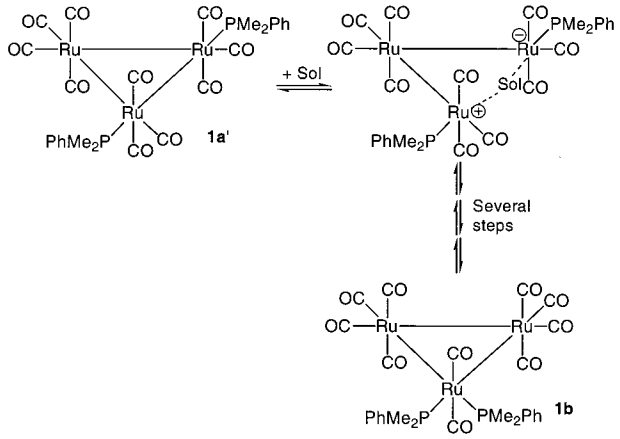

stabilize the developing positive charge, this observation is the opposite to that expected on an electronic basis and most likely signifies a steric effect.

Reactions of $Ru_3(CO)_{10}(PMe_2Ph)_2$ and $Ru_3(CO)_{10}(PPh_3)_2$ with Hydrogen. When a sample containing **1** in toluene-d_8 under 3 atm of *p*-H_2 is monitored by ^{1}H NMR spectroscopy at 296 K, the resulting spectrum (see Figure 3) contains four enhanced hydride resonances at δ −10.37, −11.10, −18.15, and −18.61 (the NMR data for these products are listed in Table 3). The chemical shifts of these hydride resonances suggest that the first two arise from terminal hydride ligands and the second two arise from bridging hydride ligands.[30] Since the signals at δ −11.10 and −18.15 are connected in a COSY experiment, they originate from the same product; the δ −10.37 and −18.61

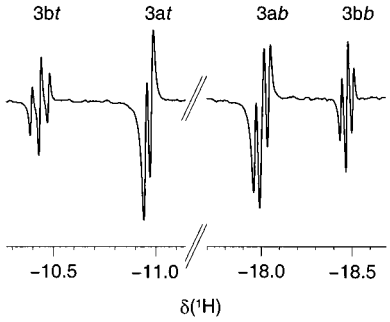

Figure 3. ^{1}H NMR spectrum showing the enhanced hydride resonances obtained for **3** when it is generated from the reaction of **1** with *p*-H_2 in benzene-d_6 at 296 K.

signals were connected in a similar way. Careful examination of the hydride resonance at δ −18.15 (**3a***b*, where the label **3a** indicates the complex, and the *b* that it is in a bridging position) revealed, in addition to a hydride−hydride coupling of −6.8 Hz, the presence of extra couplings to two different phosphorus centers (J_{PH} values 13.8 and 18.2 Hz).[44] However, the partner that resonates at δ −11.10 (**3a***t*, *t* indicates terminal) only coupled to a single ^{31}P center with a J_{PH} coupling of 12.5 Hz being indicative of a cis hydride−phosphine arrangement.[30] This suggests that **3a** contains the $(PMe_2Ph)(H)Ru(\mu\text{-}H)Ru(PMe_2Ph)$ subunit as shown in Figure 4. Both sets of hydride resonances for isomer **3b** are split into triplets by two apparently equivalent ^{31}P nuclei. Consequently, the two phosphine ligands are inequivalent and located on the same Ru center in a $(PMe_2Ph)_2(H)Ru(\mu\text{-}H)Ru$ arrangement with the ^{1}H−^{31}P coupling of 16.4 assigned to the terminal hydride and the 13.0 Hz coupling to the bridging hydride as determined via suitable coupling-selective HMQC observations. In view of fact that we see apparently equivalent ^{31}P couplings from two phosphine centers to each hydride ligand, this situation requires careful examination.[30] If the phosphine ligands are exchanging positions, the spectra would contain the average of the two distinct J_{PH}

(41) Throughout the text, the use of the symbol **a** to identify a compound (e.g., in **1a** or **2a**) refers to the time-averaged NMR signal observed at higher temperatures for isomers **a′**, **a″**, and **a‴**. See Figure 1 for structures.

(42) McAuliffe, C. A.; Levason, W. In *Phosphine, Arsine and Stilbene Complexes of the Transition Elements*; Elsevier Scientific Publishing Co.: Amsterdam, 1979.

(43) Johnson, B. F. G.; Roberts, Y. V. *Polyhedron* **1993**, *12*, 977.

(44) Aime, S.; Gobetto, R.; Valls, E. *Inorg. Chim. Acta* **1998**, *275*, 521.

Table 3. NMR Data for Hydrogen Addition Products **3** (toluene-d_8 at 296 K) and **4** (toluene-d_8, 253 K) (See Figure 6 for Positions of P_A and P_B)

compd	^{1}H	^{31}P	^{13}C
3a	(**3a***t*) −11.10, dd (J_{PAH} = 12.5 Hz, J_{HH} = −6.8 Hz)	14.4, s (P_A), −4.8, s (P_B)	201.5, d (J_{CC} = 5.6 Hz, J_{CC} = 5.6 Hz), 206.5, d (J_{CC} = 5.6 Hz)
	(**3a***b*) −18.15, ddd (J_{PBH} = 13.8 Hz, J_{PAH} = 18.2 Hz, J_{HH} = −6.8 Hz)		197.0, d (J_{CC} = 1.4 Hz), 204.0, t (J_{CC} = 1.4 Hz)
3b	(**3b***t*) −10.37, td (J_{PH} = 16.4 Hz, J_{HH} = −4.5 Hz)	−0.6, s	202.0, s
	(**3b***b*) −18.61, td (J_{PH} = 13.0 Hz, J_{HH} = −4.5 Hz)		194.5, t (J_{CC} = 2.7 Hz), 204.5, t (J_{CC} = 2.7 Hz)
4a	(**4a***t*) −10.11, d (J_{PH} = 11.0 Hz)	44.2, s (P_A), 31.2, s (P_B)	
	(**4a***b*) −17.47, dd (J_{PBH} = 10.2, J_{PAH} = 20.5 Hz)		
4b	(**4b***t*) −11.19, unknown multiplicity		
	(**4b***b*) −17.37, unknown multiplicity		

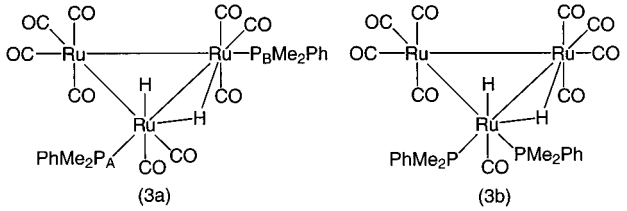

Figure 4. Structures of (a) **3a** and (b) **3b** as revealed by ^{1}H, ^{31}P, and ^{13}C NMR data.

couplings. For **3a**, the J_{PH} value corresponding to the Ru based (bridging-hydride) − (terminal phosphine) connection is 18.2 Hz, while for **3b** the time-averaged coupling is 13.0 Hz. Since the time-averaged coupling is less than 18.2 Hz, the 18.2-Hz coupling must arise from a *trans*-(P)Ru(μ-H) arrangement since this yields the largest J_{PH} value. The chemical shifts for the phosphine ligands of **3a** and **3b** were located using a 2D ^{1}H−^{31}P HMQC experiment. While two ^{31}P signals were found for **3a** at δ 14.4 and −4.8, only one was located for **3b** at δ −0.6 (toluene-d_8). From the structures in Figure 4, **3b** should contain a pair of inequivalent phosphines located on a single ruthenium center, which are always magnetically distinct in the context of their interaction with the hydride ligands. Since close examination of the ^{31}P signal for **3b** failed to split the δ −0.6 resonance and the hydride resonances are first order in appearance, we can reliably deduce that the two phosphines interchange their positions rapidly at 296 K.

From these data, it is not unreasonable to assume that **1a** and **1b** have the same basic structure as that of their hydrogen adducts, i.e., one phosphine ligand on each of two separate Ru atoms for **1a** and two phosphine ligands on the same Ru for **1b**. To explore this further, **1** was labeled with ^{13}CO, viz. **1**-^{13}C, and analyzed by ^{13}C NMR spectroscopy. The ^{13}C NMR spectrum of the precursor **1**-^{13}C, in toluene-d_8, contained only three signals due to carbonyl ligands at δ 196.2, 207.7, and 211.5. These signals were still substantially broadened due to dynamic effects and possessed no fine structure that could be attributable to ^{31}P splittings. This result is not surprising considering the widely reported carbonyl fluxionality of $M_3(CO)_{12}$ clusters and their derivatives, where M = Fe,[45] Ru,[46] or Os.[47] Analogous behavior has also been reported for the carbonyl ligands of $H_2Os_3(CO)_{10}$ and its derivatives.[48] Rapid interchange of the phosphine ligands in **3b** is therefore not totally unexpected.

To characterize more fully the hydrogen addition products, the reaction of *p*-H_2 with a benzene-d_6 solution of **1**-^{13}C was examined. The enhanced hydride resonances now showed visible couplings to ^{13}C when compared with signals obtained from a sample with ^{13}CO present at natural levels (see Figure 5a and b). For the low-field hydride resonances, the ^{1}H−^{13}C coupling of 12.5 Hz (obtained by simulation) is indicative of a trans ^{1}H−^{13}CO arrangement.[46] A series of ^{1}H−^{13}C HMQC spectra were recorded in order to locate the associated carbonyl carbon signals. A typical spectrum is illustrated in Figure 5c. Spectra were optimized for each ^{13}C resonance by changing the associated delays to account for the different values of cis and trans $^2J(^{13}C-^1H)$ and changing the spectral center to match the desired resonance's chemical shift (see Table 3). For example, when a $^2J(^{13}C-^1H)$ value of 12.5 Hz was employed, strong connections were visible to peaks at δ 201.5 from **3a***t* and δ 197.0 from **3a***b*. For a value of 2.5 Hz, corresponding to a cis coupling, connections from **3a***t* appear to a peak at δ 206.5 and from **3a***b* to a peak at δ 204.0.

It was possible to assign structures to **3a** and **3b** by assuming they have 48-valence electrons. For example, the hydride resonance due to **3b***t*-^{13}C is split by a 12.5 Hz coupling to one carbonyl carbon. The ^{1}H−^{13}C{^{31}P} HMQC located the associated ^{13}C resonance as a singlet at δ 202.0 and since it does not couple to any other carbonyl group on that metal center it is unique. The hydride and the carbonyl must therefore adopt axial positions with respect to each other, with the two phosphine ligands located at the remaining two sites in the equatorial plane. The associated bridging hydride **3b***b* was found to interact with four carbonyls on the second Ru center as evidenced by the two sets of ^{13}C resonances that are each split into triplets due to couplings to the two additional ^{13}CO ligands. These signals arise from pairs of apparently equivalent axial and equatorial carbonyl ligands and the structure **3b** shown in Figure 4 is indicated. A similar solid-state structure has been reported for substituted $H_2Os_3(CO)_{10}L$ clusters.[49]

By using a similar process, the structure of **3a** was assigned (see Table 3 and Figure 4). In brief, the hydride resonance **3a***t*-^{13}C shows an extra 12.5 Hz splitting due to a trans carbonyl carbon which resonates at δ 201.5 and is split into a doublet by coupling to a second ^{13}CO ligand (located as a doublet at δ 206.5). The latter carbonyl is located in the equatorial plane and the remaining position is occupied by the phosphine. Similar connections from the bridging hydride **3a***b* to the ligands on

(45) (a) Mann, B. E. *J. Chem. Soc., Dalton Trans.* **1997**, 1457. (b) Johnson, B. F. G. *J. Chem. Soc., Dalton Trans.* **1997**, 1473.

(46) Aime, S.; Dastru, W.; Gobetto, R.; Viale, A. *Organometallics* **1998**, *17*, 3182.

(47) (a) Deeming, A. J.; Donovan-Mtunzi, S.; Kabir, S. E. *J. Organomet. Chem.* **1985**, *281*, C43. (b) Deeming, A. J.; Donovan-Mtunzi, S.; Kabir, S. E.; Manning, P. J. *J. Chem. Soc., Dalton Trans.* **1985**, 1037.

(48) Aime, S.; Osella, D.; Milone, L.; Rosenberg, A. *J. Organomet. Chem.* **1981**, *213*, 207.

(49) Keister, J. B.; Shapley, J. R. *Inorg. Chem.* **1982**, *21*, 3304.

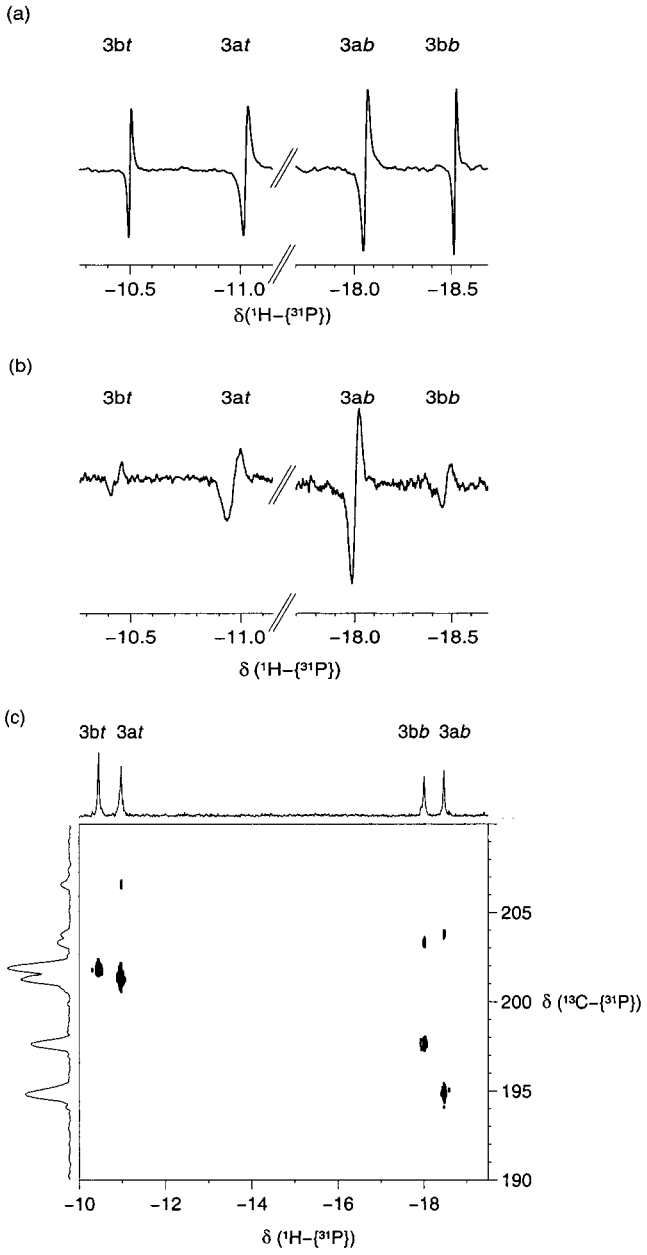

Figure 5. *p*-H_2 enhanced NMR spectra of **3** in benzene-d_6 at 296 K: (a) $^1H\{^{31}P\}$ spectrum of an unlabeled sample, (b) $^1H\{^{31}P\}$ spectrum of a ^{13}C-labeled sample revealing enhanced peak separations due to $^1H-^{13}C$ couplings, and (c) selected cross-peaks (absolute value display) and projections showing hydride and carbonyl chemical shift connections in a typical $^1H-^{13}C\{^{31}P$-decoupled$\}$ HMQC spectrum.

the second Ru center reveal the presence of one equatorial and two axial carbonyls. Collectively, these data support the structures for **3a** and **3b** shown in Figure 4.

We note that the carbonyl and phosphine ligands in the equatorial plane of **3b** either have coincident chemical shifts or rapidly interchange their positions while maintaining their location on the same ruthenium center. Since the bridging hydride resonance in **3b** appears as a triplet rather than a second-order multiplet, chemical shift coincidence can be excluded and averaging of the inequivalent cis and trans J_{P-H} couplings must occur. It is possible that a similar process facilitates interchange within **1a**. Furthermore, since the intensity of the cross-peaks observed in the HMQC spectra is controlled by the delay used for coherence transfer, exchange between equatorial and axial sites, if present, must occur on a much slower time scale.

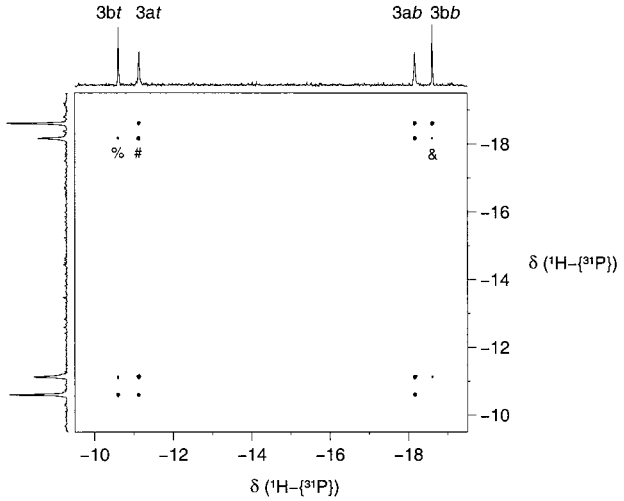

Figure 6. 2D $^1H\{^{31}P$-decoupled$\}$ EXSY spectrum (positive contours) of a sample of **3** with *p*-H_2 in toluene-d_8 at 301 K for a mixing time of 0.4 s. Exchange peaks connecting the hydride resonance of **3a***b* to **3a***t* (#), **3b***t* (%), and **3b***b* (&), visible with a mixing time of 0.4s, are indicated.

Reaction of **2** with *p*-H_2 in toluene-d_8 enabled the corresponding hydrogen addition products **4** to be detected. However, the exchange between the hydrides and free hydrogen was too slow for PHIP enhancements to be observed at 253 K, and normal signals were seen. Pairs of terminal and bridging hydrides were observed (**4a***t*, **4a***b*, **4b***t*, **4b***b*), suggesting that products analogous to **3a** and **3b** are formed. While the data for **4a** clearly demonstrate that it contains one phosphine ligand on each of two Ru atoms, as well as a terminal and bridging hydride, the signals for **4b** were much weaker and their multiplicities could not be determined. The spectral data for **4** are summarized in Table 3. Above 265 K, the exchange rate for hydrogen addition/reductive elimination is such that small PHIP enhancements are first observed, and at even higher temperatures the associated resonances become extremely broad.

Upon removal of the H_2 atmosphere **3** and **4** disappear over a period of ∼30 s. When the [H_2] (toluene-d_8, 301 K) present in solution in a sample of **1** was increased by a factor of 2.15, the ratios of **3a** to **1a** and **3b** to **1b** changed dramatically. The ratio ([**1a**][H_2])/([**3a**][CO]) was determined to be $(2.3 \pm 0.6) \times 10^{-4}$ for both [H_2]. Similarly, the corresponding ratio for the reaction **1b** + $H_2 \rightarrow$ **3b** + CO was determined as $(9.7 \pm 1) \times 10^{-5}$. Assuming that these ratios correspond to equilibrium constants, the corresponding free energy differences for **1a**/**3a** and **1b**/**3b** are 21 ± 1 and 23 ± 1 kJ mol^{-1}, respectively. These free energy differences are illustrated in Figure 2.

Ligand Exchange Pathways in $(H)_2Ru_3(CO)_9(PMe_2Ph)_2$ and $(H)_2Ru_3(CO)_9(PPh_3)_2$. EXSY spectroscopy has been used to follow the dynamic behavior of the hydride ligands in **3a** and **3b**, and a typical spectrum is shown in Figure 6. The observation of positive exchange cross-peaks between *all* the hydride resonances of **3a** and **3b** at longer mixing times indicates that *all* the hydride ligands are able to exchange positions. Exchange with free H_2 is not observed on this time scale.

EXSY spectra were recorded for a variety of mixing times, temperatures. and solvents and the resultant data analyzed according to the procedure outlined in the Experimental Section.[37] For example, when EXSY spectra were recorded at 301 K for **3**, the raw data shown in Table 4 were obtained. The data presented illustrate the correlation between measured and calculated peak areas for exchange of **3a***t* into **3a***b* and **3b***t* and **3b***b*, as illustrated in Figure 7a. The rate constants obtained for

Table 4. EXSY Data for Hydride Interchange from Location **3a***t* into Locations **3a***b*, **3b***t*, and **3b***b* at 301 K[a]

mixing time τ_{mix} (s)	measured/calculated [**3a***t*]	[**3a***b*]	[**3b***t*]	[**3b***b*]	Σ^2 [measd − calcd]
0	100/100	0/0	0/0	0/0	0
0.05	65.3/65.0	34.7/32.2	0/0.9	0/1.8	10
0.075	62.0/57.5	38.0/38.6	0/1.5	0/2.5	29
0.1	55.5/52.9	44.5/42.0	0/2.0	0/3.1	27
0.3	43.4/44.0	39.2/43.9	7.3/5.7	10.0/6.5	41
0.5	37.4/41.8	44.0/41.8	9.7 /8.0	8.9/8.5	26
0.6	38.8/41.0	42.6/41.1	9/8.7	9.6/9.2	8
minimized value: $\Sigma^2_{all}\,\tau_{mix}$ [measd − calcd]					141

[a] tabulated data include measured and calculated peak areas for specified mixing times, together with indicators of goodness of fit.

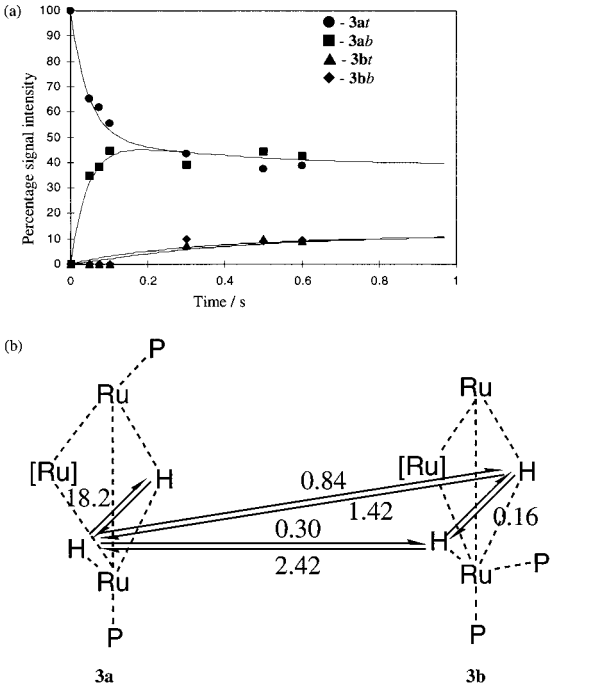

Figure 7. (a) Simulated (solid line) and experimental data (♦, ●, ■, ▲) for the exchange processes involving site **3a***t* in toluene-d_8 at 301 K and (b) schematic diagram for complex **3** showing the exchange rate constants at 301 K. (The ligands on the third ruthenium center are omitted for clarity.)

these processes at 301 K are shown in Figure 7b. Repeating this procedure over the temperature range 273−312 K enabled the activation parameters $\Delta H^{\ddagger}$ and $\Delta S^{\ddagger}$ to be obtained for these pathways.

It should be noted that although a large temperature range was used, not all the processes could be followed over the full range. For example, while the intramolecular hydride exchange for the major species **3a** could always be reliably followed, exchange between the isomers was too slow at the lower temperatures, and too fast at the higher temperatures, to be monitored accurately. Furthermore, since the minor isomer **3b** could only be detected readily at high temperatures, little data were available for processes starting from **3b**. These limitations constrained the available rate data and consequently widened the confidence limits of the associated activation parameters. The activation parameters for processes i, iii, and iv were determined reliably and are presented in Table 5.

It is noteworthy that intraisomer exchange in **3a** corresponds to the fastest process, with the terminal hydride **3a***t* moving into position **3a***b* at a rate of 18.2 s^{-1} in toluene-d_8 at 301 K.

Table 5. Activation Parameters for Identified Hydride Exchange Processes in Species **3a** and **3b**

process	toluene-d_8	$CDCl_3$
3a*b* → **3a***t* and **3a***t* → **3a***b*		
$\Delta H^{\ddagger}$ (kJ mol^{-1})	30 ± 8	49 ± 4
$\Delta S^{\ddagger}$ (J K^{-1} mol^{-1})	−122 ± 26	−57 ± 14
3a*b* → **3b***b* and **3a***t* → **3b***t*		
$\Delta H^{\ddagger}$ (kJ mol^{-1})	150 ± 12	
$\Delta S^{\ddagger}$ (J K^{-1} mol^{-1})	242 ± 37	
3a*b* → **3b***t* and **3a***t* → **3b***b*		
$\Delta H^{\ddagger}$ (kJ mol^{-1})	51 ± 8	
$\Delta S^{\ddagger}$ (J K^{-1} mol^{-1})	−76 ± 24	

On a slower time scale, interisomer interchange occurs, with **3a***t* moving into the terminal position **3b***t* at a rate of 0.30 s^{-1} and into the bridging position **3b***b* at a rate of 0.84 s^{-1}. The reverse processes are much faster, in keeping with the dominance of isomer **3a**. At 301 K, the rate constant for interchange of the precursor **1a** into **1b** is 62.1 s^{-1}. This process therefore occurs on a much faster time scale than intraisomer hydride interchange in **3a**.

The rate of hydride exchange within **3a** was unaffected (within experimental error) by CO although the observed rate constants for **3a***t* → **3b***t* and **3a***b* → **3b***b* were both dramatically reduced. Unfortunately no data could be collected for the effect of phosphine since immediate conversion to $Ru_3(CO)_9(PMe_2Ph)_3$ occurred.[30]

The bridge ↔ terminal exchange process in **3a** has a relatively small enthalpy of activation ($\Delta H^{\ddagger}$ = 30 kJ mol^{-1} in toluene-d_8) and a substantially negative entropy term ($\Delta S^{\ddagger}$ = −122 J K^{-1} mol^{-1}). As such, solvent participation in this step is sizable. A concerted motion of hydride and carbonyl ligands has been proposed to account for the hydride interchange in $H_2Os_3(CO)_{11}$ and its derivatives.[49,50] However, such motion is unlikely here since the solvent effect would be minimal. Homolysis of a ruthenium−ruthenium bond is also unlikely since this would quench the *p*-H_2 enhancement.[51] It is therefore conceivable that the mechanism involves rate-determining heterolysis of the hydride-bridged Ru−Ru bond, with concurrent formation of a 16-electron metal dihydride cation and an 18-electron anion, followed by reversible formation of an η^2-H_2 ligand, rotation, and closure (see Scheme 2a). For this process, the low-polarity solvent toluene promotes exchange when compared to the more polar $CDCl_3$. Rate-limiting solvent displacement from the solvated intermediate is consistent with the data. The role of η^2-H_2 ligands in the oxidative addition of H_2 is well established.[52]

By microscopic reversibility,[53] the same rationale can be extrapolated to postulate a pathway for hydrogen addition to **1a**. Thus, oxidative addition of H_2 occurs to the 16-electron center produced after heterolytic scission of the Ru−Ru bond. Subsequent CO loss, and reestablishment of the Ru−Ru bond, as shown in Scheme 2b, leads to the final product.

The interisomer exchange process where the hydrides of the major and minor isomers remain in the same relative positions (i.e., **3a***t* → **3b***t* and **3a***b* → **3b***b*) yielded $\Delta H^{\ddagger}$ = 150 kJ mol^{-1} and $\Delta S^{\ddagger}$ = 242 J K^{-1} mol^{-1} in toluene-d_8. The large positive entropy term suggests that this process involves ligand dissociation. This conclusion is supported by the dramatic reduction in observed rate for this process when CO is added to the system.

(50) Aime, S.; Osella, D.; Milone, L.; Rosenberg, E. *J. Organomet. Chem.* **1981**, *213*, 207.
(51) Eisenberg, R. *Acc. Chem. Res.* **1991**, *24*, 110.
(52) (a) Heinecke, D. M.; Oldhem, W. J. *Chem. Rev.* **1993**, *93*, 913. (b) Jessop, P. G.; Morris, R. H. *Coord. Chem. Rev.* **1992**, *121*, 155.
(53) Jones, W. D.; Feher, F. J. *Acc. Chem. Res.* **1989**, *22*, 91.

Scheme 2. (a) Proposed Hydride Exchange Mechanism for the Process **3a***t* → **3a***b* and (b) Proposed Mechanism of Hydrogen Addition to **1a**″

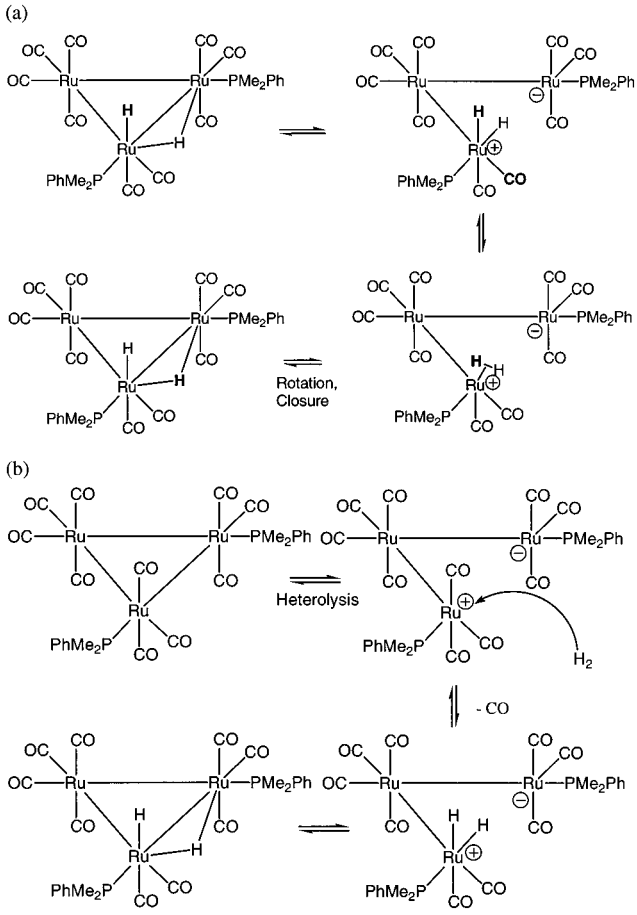

CO ligand loss can occur directly from **3a** or from the intermediate formed after Ru−Ru bond heterolysis. Subsequent steps, including phosphine migration, are necessary to complete the exchange. For example, if the carbonyl ligand illustrated in boldface type in Scheme 2a dissociates, transfer of the phosphine from the remote ruthenium center into the vacant coordination site and recoordination of CO complete this process.

The exchange from the major to the minor isomer with interchanging hydride positions (i.e., **3a***t* → **3b***b* and **3a***b* → **3b***t*) is the last process for which meaningful kinetic data could be extracted. The kinetic analysis required that this interconversion be distinct from that which is achieved by the product of the first two processes. This second, slower and direct route yielded values for $\Delta H^{\ddagger}$ of 51 kJ mol^{-1} and for $\Delta S^{\ddagger}$ of −76 J K^{-1} mol^{-1} in toluene-d_8. Given the negative entropy of activation, it is surprising that added CO also inhibited this process. Clearly, if both the isomer interchange pathways involve a common intermediate formed by CO loss, the rate-determining step for the conversion **3a***t* → **3b***b* is significantly different from that involved in conversion **3a***t* to **3b***t*. At this stage, we are unable to speculate further about the exact nature of this process. No rate data are presented for interconversions involving **4** because these products could not be detected with sufficient signal strengths to facilitate their analysis.

Conclusions

In this paper, we have shown that clusters $Ru_3(CO)_{10}(PMe_2Ph)_2$ **1** and $Ru_3(CO)_{10}(PPh_3)_2$ **2** exist in solution in at least three distinct isomeric forms. The minor isomer contains both phosphines on the same ruthenium center in the equatorial plane, and the others have phosphines in the equatorial plane on different ruthenium centers. The isomers were shown to interconvert by EXSY spectroscopy and line shape analysis. High levels of solvent participation and associated change in activation parameters indicate that phosphine movement between ruthenium centers proceeds via initial heterolysis of a Ru−Ru bond with the intermediates being stabilized by the solvent. The effect of the solvent is found to be much greater for the PMe_2Ph-substituted cluster than for the PPh_3 analogue, an effect that can be attributed to the bulk of the PPh_3 ligand preventing the solvent from interacting with the Ru−Ru bond during heterolysis.

Both these clusters have been shown to react with hydrogen. NMR spectroscopy, in conjunction with para hydrogen-induced polarization, has allowed the determination of the structures of the two products of hydrogen addition to **1** as H(μ-H)$Ru_3(CO)_9(PMe_2Ph)_2$ **3** (see Figure 4). Hydrogen addition is suggested to proceed via oxidative addition to the 16-electron center formed after the heterolysis of the Ru−Ru bond, followed by loss of CO and closure of the Ru−Ru bond. Removal of the H_2 atmosphere results in rapid re-formation of the precursor clusters. These four species are connected via a suitable free energy plot (see Figure 2), with the Ru^0 precursors being the most stable.

The two isomers of the hydrogen addition product have been shown to interconvert, and the kinetic data suggest that intramolecular hydride exchange within the major isomer, which contains a $(PMe_2Ph)(H)Ru(\mu\text{-}H)Ru(PMe_2Ph)$ arrangement, proceeds via Ru−Ru bond heterolysis followed by formation of an η^2-H_2 ligand, rotation about the Ru−H_2 bond, and closure. Two slower processes, comprising exchange between the above isomer and one containing a $(PMe_2Ph)_2(H)Ru(\mu\text{-}H)Ru$ arrangement have been detected and are shown to involve CO loss.

Acknowledgment. D.B. acknowledges financial support from the ORS Award Scheme. S.B.D. is grateful to the University of York, the EPSRC, the JREI scheme, and Bruker UK (sponsorship and spectrometer) for financial support. P.J.D. thanks the Royal Society for a University Research Fellowship. Discussions with Prof. R. Eisenberg (NATO support), Prof. R. N. Perutz, and Dr. R. J. Mawby are gratefully acknowledged.

Supporting Information Available: Additional details as indicated in text. This material is available free of charge via the Internet at http://pubs.acs.org.

JA004245N